Water Science & Technology

IWA PUBLISHING

Water Science & Technology Vol 84 No 9, 2472 doi: 10.2166/wst.2021.440

Permeable reactive barrier of waste sludge from wine processing utilized to block a metallic mixture plume in a simulated aquifer

Shui-Wen Chang Chien[a], Yi-Pei Li[b] and Cheng-Chung Liu[b,*]

[a] Department of Environmental Engineering and Management, Chaoyang University of Technology, Taichung 41349, Taiwan
[b] Department of Environmental Engineering, National Ilan University, Ilan 26047, Taiwan
*Corresponding author. E-mail: ccliu@niu.edu.tw

ABSTRACT

Heavy metal contamination in underground water commonly occurs in industrial areas in Taiwan. Wine-processing waste sludge (WPWS) can adsorb and remove several toxic metals from aqueous solutions. In this study, WPWS particles were used to construct a permeable reactive barrier (PRB) for the remediation of a contaminant plume comprising $HCrO_4^-$, Cu^{2+}, Zn^{2+}, Ni^{2+}, Cd^{2+}, and AsO_3^{3-} in a simulated aquifer. This PRB effectively prevented the dispersals of Cu^{2+}, Zn^{2+}, and $HCrO_4^-$, and their concentrations in the pore water behind the barrier declined below the control standard levels. However, the PRB failed to prevent the diffusion of Ni^{2+}, Cd^{2+}, and AsO_3^{3-}, and their concentrations were occasionally higher than the control standard levels. However, 18% to 45% of As, 84% to 93% of Cd, and 16% to 77% of Ni were removed by the barrier. Ni ions showed less adsorption on the fine sand layer because of the layer's ineffectiveness in multiple competitive adsorptions. Therefore, the ions infiltrated the barrier at a high concentration, which increased the loading for the barrier blocking. The blocking efficiency was related to the degree of adsorption of heavy metals in the sand layer and the results of their competitive adsorption.

Key words: aquifer, heavy metals, permeable reactive barrier, sludge

HIGHLIGHTS

- A wine-processing waste sludge (WPWS) permeable reactive barrier (PRB) successfully prevented the spread of $HCrO_4^-$, Cu^{2+}, and Zn^{2+}.
- WPWS PRB had an extremely high affinity to $HCrO_4^-$.
- WPWS PRB had a low affinity to AsO_3^{3-}.
- Multiple competitive adsorption results showed WPWS PRB as a poor block to Ni^{2+}.
- Adsorption from sand layer to metals also affected the block efficiency.

INTRODUCTION

The Environmental Protection Administration, Executive Yuan, discovers more than ten toxic-metal contamination sites each year through routine investigations of groundwater in all large-scale industrial districts of Taiwan. Spontaneous seepage of chemicals and illegal disposal of industrial wastewater into the soil are considered to be the major causes for these pollution incidents. Factories and manufacturing units commonly utilize large metallic tanks to store chemicals. Complicated pipeline systems have been constructed to transfer such chemicals. Once cathodic corrosion occurs (Okyere 2019), the chemicals, containing high concentration of heavy metals, can seep from the underground tanks or pipelines and probably reach the aquifer within a short time period, as long as they flow along the soil cracks (Hillel 1999). However, negatively charged soil minerals can strongly adsorb the transition elements; that is, Cr^{3+}, Cu^{2+}, Zn^{2+}, Ni^{2+}, and Cd^{2+}, and inhibit their mobilization (Logan 1999). Heavy metal anions, such as $HCrO_4^-$ and AsO_3^{3-}, are more easily leached into the aquifer, thereby causing greater harm to the environment (Ahuja 2008; Komárek *et al.* 2013; Chen *et al.* 2019). Contamination of groundwater with heavy metals is usually caused by numerous industrial applications, such as the production of alloys and stainless steel (Yuan *et al.* 2014), electroplating (Wei *et al.* 2013), leather tanning (Nur-E-Alam *et al.* 2020), pigmentation, and wood preservation (Rent *et al.* 2017). Additionally, in the United States, more than 90% of the total arsenic consumption is for agricultural purposes. This includes the production of wood preservatives (74% of total), herbicides, insecticides, fungicides, desiccants, antiparasitic medications, and growth stimulants for plants and animals (Agency for Toxic Substances and

Disease Registry 2007). In Taiwan, arsenic pollution in groundwater was only caused by an illegal dumping and burial from a specific pesticide manufacturing plant.

Toxicity of heavy metals is attributed to their good solubility in water, long biological half-lives, and propensity towards bioaccumulation. Accumulation of heavy metals in different body tissues has the potential to affect vital organs such as kidneys, bones, and liver, and can cause serious health hazards (Wu 2020). The threshold levels for Cd^{2+}, $HCrO_4^-$ and AsO_3^{3-} in standards for drinking water are very low compared to some other elements because these compounds are highly toxic to living organisms. They have been classified as a Group A human carcinogen by the U.S. Environmental Protection Agency (Dhal *et al.* 2013; Kim *et al.* 2015).

In summary, heavy metal ions are hazardous to human health and the environment, even at low concentrations. Thus, effective remediation technologies to reduce the risk of spreading contaminated water plumes throughout aquifers and to decrease negative effects on the ecosystem are in high demand (Kumarasinghe *et al.* 2018). The conventional pump-and-treat method combining groundwater extraction and *ex-situ* treatment is widely used in remediating contaminated groundwater, but this option is expensive and often ineffective in meeting water quality standards (Maamoun *et al.* 2020).

Permeable reactive barriers (PRBs) have received considerable attention as a practical and cost-effective methodology for the in-situ treatment of contaminated groundwater in recent years (Obiri-Nyarko *et al.* 2014). Using natural water flow, the installation of a PRB downstream of the contaminant plume enables the trapping of pollutants and minimizes the spread of pollutants. The major advantage of PRB technology is that it utilizes natural groundwater flow to transport pollutants toward the reactive materials without requirements for an energy input or above-ground facilities (Gavaskar 1999; Snape *et al.* 2001). An important consideration in PRB design is the selection of the reactive material. Various adsorbent media, including zero-valent iron (Henderson & Demond 2007; Chen *et al.* 2011; Singh & Singh 2018; Hu *et al.* 2019b), zero-valent aluminum (Han *et al.* 2016), zeolite (Statham *et al.* 2016), fly ash (Czurda & Haus 2002), biochar (Hu *et al.* 2019a), activated carbon (Liu *et al.* 2012b; Singh & Singh 2018), waste green sand, peat (Guerin *et al.* 2002; Erto *et al.* 2011), and even mixed adsorbents (Kumarasinghe *et al.* 2018; Mittal *et al.* 2021) are widely used in groundwater remediation. PRB is considered a practical approach to treat heavy metal ions that contaminate subsurface water owing to its low cost, high efficiency, and environmental friendliness (Dong *et al.* 2009). However, treating co-existing heavy metal ions is difficult, especially when heavy metal ions coexist in the form of cations and anions (Han *et al.* 2016).

Hualien Winery & Distillery produces approximately 300 tons of waste sludge a month from the final clarifier and settling basin of the wastewater treatment process. The waste removal fee is a considerable operating cost. However, the abundant organic material and high binding affinities of wine-processing waste sludge (WPWS) make it a useful adsorbent for the removal of cationic pollutants from aqueous solutions (Liu *et al.* 2005; Liu *et al.* 2006; Liu *et al.* 2009). The C/N ratio of WPWS ranged from 5:1 to 10:1, indicating that it is a mature and stable material that does not stink. WPWS has previously been used to build a new type of PRB, termed WPWS PRB, to block a gasoline plume in a simulated aquifer, and an extraordinary removal rate was achieved (Liu *et al.* 2020). However, few studies have simultaneously remediated disparate contaminants using PRB. The purpose of this study was to assess the effectiveness of utilizing the WPWS PRB to treat a mixed metal plume comprising Cu^{2+}, Zn^{2+}, Ni^{2+}, Cd^{2+}, $HCrO_4^-$, and AsO_3^{3-}, in a simulated aquifer. The interception efficiency of the WPWS PRB was evaluated, and the distribution of the tested metals in the PRB was revealed.

METHODS

Preparation of wine-processing waste sludge from winery

The utilized WPWS was collected from a wastewater treatment plant in Hualien Winery & Distillery. It was dried at room temperature, ground, and sieved through 16- and 35-mesh sieves. Then, WPWS particles were mixed evenly using a machine and stored in cans. Finer particles were not considered for PRB because the sludge particles undergo a restricted swelling when they soak in water for several days, which would likely cause the barrier to block itself. An analysis of the chemical properties of WPWS was conducted to determine the major elements, pH, cation exchange capacity (CEC), and organic matter content. The total C, H, N, S, and O contents were evaluated using an auto elemental analyzer (vario EL cube), and K, Ca, Mg, Fe, Al, Mn, and P contents were determined via energy-dispersive spectrometry (Kevex level 4). The pH was measured at a 1:5 ratio of WPWS to water using a pH meter. The organic matter content was obtained by multiplying 1.724 by the carbon content from the wet oxidation method (Walkley & Black 1934). The cation exchange capacity of WPWS

was determined using a conventional ammonium-sodium exchange method (Avom *et al.* 1997). All the experiments about the characteristics of WPWS were performed in duplicate.

Experiment for mixed plume of heavy metals blocked by WPWS PRB

A transparent acrylic water tank (external size of 106 cm × 50 cm × 100 cm) was used to simulate the heavy-metal plume blockage in the aquifer of the WPWS PRB. The distributions of the first sand zone, reactive barrier, second sand zone, and inlet/outlet water chambers in the water tank are presented in Figure 1. The sand layer, which was divided into two sections by the PRB, was located in the middle of the water tank and had a total length of 135 cm and a filling height of 80 cm. The WPWS PRB was located downstream of the plume, traversing the entire tank with a height of 80 cm, the same as the sand layer, and a thickness of 10 cm. Its filling mass was 49.9 kg, and the bulk density was 1.25 g cm^{-3}. The depth of the aquifer layer was a constant 70 cm. To assess the effectiveness of the WPWS PRB in intercepting heavy metals, a sampling point was set at the center point 3 cm downstream from the PRB. Three glass tubes of various lengths (inner diameter R = 6.0 mm, outer diameter R = 6.3 mm) were buried at the sampling point to collect pore water: one near the top of the aquifer layer (1 cm below the water table), one at the middle of the aquifer layer (35 cm from the tank bottom), and one near the bottom of the aquifer layer (1 cm from the tank bottom). In contrast, another sampling point was established 3 cm upstream from the WPWS PRB to monitor the residual amounts of heavy metals in the sand layer. Three glass tubes with different lengths were also set for the three sampled water depths, similar to the other point. This was useful for determining the end time of the experiment. The sand layer porosity was approximately 0.45. A heavy metal mixture solution was prepared

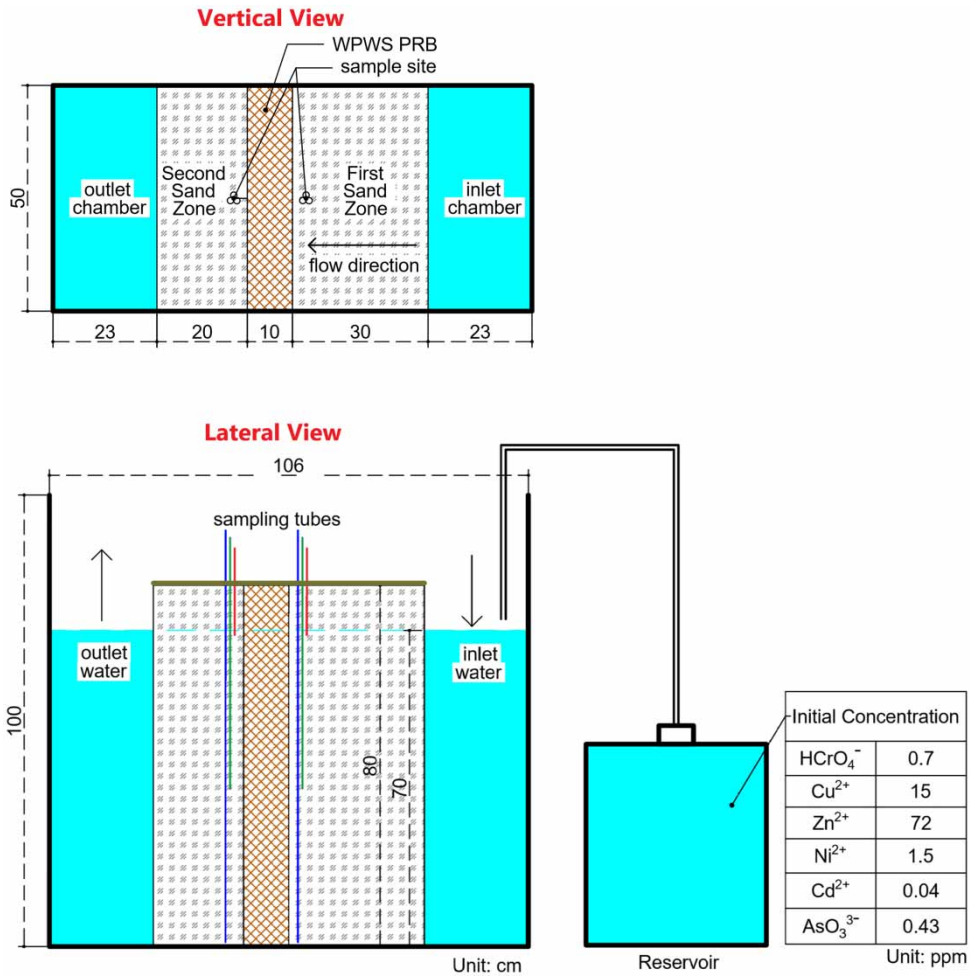

Figure 1 | Components used in the water tank WPWS PRB blocking investigation and the sampling zones in the WPWS PRB.

and stored in a huge plastic tank with a pH of 5.0. Their initial concentrations were 0.25, 5, 25, 0.5, 0.025, and 0.25 mg/L for Cr ($HCrO_4^-$), Cu^{2+}, Zn^{2+}, Ni^{2+}, Cd^{2+}, and As (AsO_3^{3-}), respectively; these concentrations represent five times the control standard levels for groundwater quality. The water tank was initially filled with running water. During the experiment, two peristaltic pumps were utilized to adjust the flow rate of the system, maintained at 100 cm day^{-1}, with one to pump the metallic mixture solution from the reservoir into the tank, and the other to pump water out of the tank. Sampling downstream of the PRB was conducted every 8 h using a fine silicone tube to extend into the end of each sampling tube to draw 50 mL of pore water using a peristaltic pump. However, pore water in the first sand zone was sampled every 24 h. When the ninth sampling was completed, the running water began to replace the solution mixture pumped into the inlet chamber until the experiment was completed. This action was designed to simulate a situation in which the plume was about to pass through. The heavy metal mixture solution in the first sand zone was gradually diluted over time in this stage. Sampled water was filtered through 0.45 μm membranes, and the Cr, Cu, Zn, Ni, and Cd concentrations in the filtrates were then analyzed using a flame atomic absorption spectrometer (AAS, Hitachi Z2300, Japan). The As concentrations were determined using the same AAS equipped with a hydride generator (Hitachi HFS-3). The experiment was terminated at 176 h, and all the metal concentrations in the second sand zone decreased below the control standard levels. Average block efficiency for a pollutant was calculated by the following formulae:

$$\frac{\sum_{i=1}^{n} C_i}{n} \times 100\% \ (i = 1, 4, 7, 10, 13, 16, 19; n = 7)$$

$$C_i = \frac{\bar{C}_{b,i} - \bar{C}_{a,i+1}}{\bar{C}_{b,i}}$$

$$\bar{C}_{a,i} = \frac{C_{a,S,i} + C_{a,M,i} + C_{a,L,i}}{3}$$

$$\bar{C}_{b,i} = \frac{C_{a,S,i} + C_{a,M,i} + C_{a,L,i}}{3}$$

C_i : pollutant block rate at a specific sampling time
i: sampling order
a: sampling site before PRB
b: sampling site after PRB
$\bar{C}_{a,i}$: an average of pollutant concentration in the aquifer before PRB
$\bar{C}_{b,i}$: an average of pollutant concentration in the aquifer after PRB
Symbols S, M, and L represent sampling depth:
S (surface): below the water table of 1 cm
M (middle): half depth of the aquifer
L (low): 1 cm above the tank bottom

Distribution of heavy metals in the WPWS barrier

When the pore water flowed in the horizontal direction through the simulated aquifer, the heavy metals in the plume gradually moved downward along the water flow owing to its high density. By investigating the distribution of these metals in the WPWS PRB after the reaction's completion, the behavior of each pollutant penetrating the barrier and their migration in the aquifer were revealed. The WPWS PRB was divided into ten intervals of the same size for sample collection, from the bottom to the highest water level of the aquifer (Figure 2). Ten grams of the WPWS sample collected from the barrier was added to a 500 ml flask, and then a 35% H_2O_2 solution was used to decompose the sample's organic component at 50 °C until it was completely removed. Afterwards, the residual fraction was treated with an aqua regia solution followed by filtration. The concentrations of heavy metals in the filtrate were determined using an AAS system. The metal distribution and their penetration mechanisms for WPWS PRBs were revealed. All the experiments were conducted in duplicate.

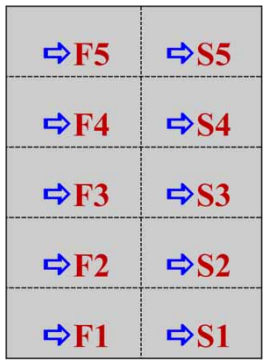

Figure 2 | Sampling zones within the WPWS PRB (F: first half area, S: second half area, ⇒flow direction).

RESULT AND DISCUSSION

Characterization of WPWS

Wine-processing waste sludge is neutral (pH 6.8). The high organic matter content (52.6%) and CEC (169 $cmol_c\ kg^{-1}$) revealed that the sludge had a large number of adsorption sites. The dominant elements in WPWS were N (3.1%),

Table 1 | Dynamics of $HCrO_4^-$ in the aquifer from the metal mixture plume (mg L^{-1})

	Site before barrier			Site after barrier		
Sampling order/time (h)	**S**	**M**	**L**	**S**	**M**	**L**
1/8	0.0255	0.0375	0.014	0.016	0.013	ND
2/16	–	–	–	0.013	ND	ND
3/24	–	–	–	ND	ND	ND
4/32	0.027	0.023	ND	0.004	ND	ND
5/40	–	–	–	0.004	ND	ND
6/48	–	–	–	0.004	0.002	ND
7/56	0.098	0.097	0.033	0.009	0.023	ND
8/64	–	–	–	0.009	ND	ND
9/72	–	–	–	0.009	0.007	ND
10/80	0.093	0.086	0.016	0.008	0.011	0.003
11/88	–	–	–	ND	ND	ND
12/96	–	–	–	ND	ND	ND
13/104	0.117	0.106	0.071	ND	ND	ND
14/112	–	–	–	ND	ND	ND
15/120	–	–	–	ND	ND	ND
16/128	0.142	0.115	0.060	ND	ND	ND
17/136	–	–	–	ND	ND	0.002
18/144	–	–	–	ND	ND	0.003
19/152	0.045	0.048	0.044	ND	ND	ND
20/160	–	–	–	ND	ND	ND
21/168	–	–	–	ND	ND	ND
22/176	–	–	–	ND	ND	0.003

Numbers with a gray background: pollutant concentrations over the control standard, 0.05 mg L^{-1}.
Sampling at 8 h intervals. Sampling site, S: below the water table of 1 cm. M: half depth of the aquifer. L: 1 cm above the tank bottom.
–: No sampling.

P (0.9%), S (3.2%), Ca (4.7%), Mg (0.4%), Na (0.25%), Fe (6.5%), Al (1.2%), Mn (0.1%), and Si (5.4%). The high Ca content originated from the lime that was employed to enhance the dehydration of the raw sludge. The Fe and Al may have originated from the coagulation reagents of the WPWS.

Investigation of heavy metals penetrating the WPWS PRB

As shown in Table 1, more than half of the sampling sites did not contain any Cr, and the Cr concentrations in the residual sites were smaller than the control standard level. A previous study revealed that $HCrO_4^-$ transforms to Cr(III) once it contacts the organic component of WPWS (Liu *et al.* 2006). However, Cr has the highest charge compared to the other tested metals; therefore, the WPWS barrier showed the best adsorption of Cr. The interception efficiency of Cu by the WPWS PRB was second only to that of $HCrO_4^-$. Minimal Cu was detected at all sampling sites during the entire reaction, and no components exceeded the control standard level (Table 2). Copper showed the highest adsorption by organic matter compared to other divalent transition elements. This is attributed to its electronic configuration and adjustable electron orbit (McBride 1989; Liu *et al.* 2011). The highest Cu concentration in the first sand zone was only 1.775 mg/L. This was still higher than the control standard but far below its concentration in the reservoir (15 mg/L), indicating that the sand layer had a significant adsorption of Cu^{2+}. As shown in Table 3, WPWS PRB also effectively diminished the dispersal of Zn^{2+}. All the Zn concentrations declined under the control standard, but most of the Zn sank or moved around the middle and bottom layers. Although previous batch experiments showed that the WPWS was poor in Zn^{2+} adsorption under a high concentration

Table 2 | Dynamics of Cu^{2+} in the aquifer from the metal mixture plume (mg L^{-1})

	Site before barrier			Site after barrier		
Sampling order/time (h)	**S**	**M**	**L**	**S**	**M**	**L**
1/8	0.640	1.177	0.629	0.050	0.080	0.264
2/16	–	–	–	0.081	0.081	0.184
3/24	–	–	–	0.089	0.137	0.273
4/32	0.891	1.196	0.497	0.079	0.028	0.034
5/40	–	–	–	0.108	0.064	0.153
6/48	–	–	–	0.029	0.084	0.148
7/56	1.250	1.775	1.012	0.137	0.575	0.098
8/64	–	–	–	0.081	0.115	0.147
9/72	–	–	–	0.166	0.245	0.201
10/80	1.258	1.487	0.583	0.073	0.136	0.243
11/88	–	–	–	0.029	0.102	0.074
12/96	–	–	–	0.025	0.085	0.071
13/104	1.173	1.439	0.854	0.030	0.075	0.065
14/112	–	–	–	0.019	0.154	0.131
15/120	–	–	–	0.027	0.066	0.044
16/128	0.471	0.871	0.366	0.022	0.112	0.153
17/136	–	–	–	0.032	0.139	0.192
18/144	–	–	–	0.011	0.023	0.026
19/152	0.309	0.707	0.274	0.017	0.050	0.081
20/160	–	–	–	0.017	0.032	0.055
21/168	–	–	–	0.013	0.019	0.050
22/176	–	–	–	0.014	0.014	0.119

Numbers with a gray background: pollutant concentrations over the control standard, 1 mg L^{-1}.
Sampling at 8 h intervals. Sampling site, S: below the water table of 1 cm. M: half depth of the aquifer. L: 1 cm above the tank bottom.
–: No sampling.

Table 3 | Dynamics of Zn^{2+} in the aquifer from the metal mixture plume (mg L^{-1})

	Site before barrier			Site after barrier		
Sampling order/time (h)	S	M	L	S	M	L
1/8	0.709	1.135	0.830	0.091	0.185	0.231
2/16	–	–	–	0.209	0.251	0.537
3/24	–	–	–	0.308	0.295	0.369
4/32	0.671	1.410	0.304	0.063	0.048	0.177
5/40	–	–	–	0.043	0.109	0.095
6/48	–	–	–	0.131	0.111	0.216
7/56	4.638	5.028	0.675	0.203	0.439	0.098
8/64	–	–	–	0.110	0.113	0.174
9/72	–	–	–	0.219	0.273	0.195
10/80	4.489	3.945	0.338	0.097	0.153	0.154
11/88	–	–	–	0.185	0.270	0.173
12/96	–	–	–	0.086	0.285	0.173
13/104	6.495	7.752	2.295	0.146	0.276	0.200
14/112	–	–	–	0.062	0.198	0.202
15/120	–	–	–	0.068	0.061	0.103
16/128	7.033	8.713	5.090	0.057	0.120	0.139
17/136	–	–	–	0.045	0.111	0.139
18/144	–	–	–	0.049	0.080	0.096
19/152	4.549	5.734	6.411	0.118	0.130	0.075
20/160	–	–	–	0.050	0.037	0.053
21/168	–	–	–	0.043	0.041	0.049
22/176	–	–	–	0.024	0.039	0.026

Numbers with a gray background: pollutant concentrations over the control standard, 5 mg L^{-1}.
Sampling at 8 h intervals. Sampling site, S: below the water table of 1 cm. M: half depth of the aquifer. L: 1 cm above the tank bottom.
–: No sampling.

(>100 mg Zn^{2+} L^{-1}), in this study, the WPWS PRB exhibited a high interception ratio of Zn^{2+} owing to adsorption under a low concentration (<15 mg Zn^{2+} L^{-1}) (Liu *et al.* 2009). The WPWS PRB absorbed 96% of the Zn imported into the system.

Ni had the lowest removal rate from the WPWS PRB (Table 4). The nickel concentration in the second sand zone reached its maximum after 8 h of processing. The high Ni concentration behind the PRB persisted until the experiment was completed. Other studies have revealed that the adsorption of Ni is far less than those of Cr and Cu under multiple competitive adsorption conditions (Liu *et al.* 2006; Liu *et al.* 2009; Liu *et al.* 2012a). At the sampling point of the first sand zone, the Ni concentrations exceeded the control standard by 4 to 6 times during most of the reaction time. We speculated that Ni adsorption was poor in the sand layer, which would increase the loading for the WPWS PRB intercepting the Ni. As shown in Table 5, Cd migration seemed to dominate in both the middle and upper sand layers. All the Cd concentrations in the first sand zone were below 0.1 mg/L; however, they were higher than 4.8 to 18.6 times the control standard level (0.005 mg/L). When the high-concentration Cd^{2+} mass flow arrived at the frontier of the PRB on the third day, excess Cd^{2+} allowed the PRB to fail in the block so that their concentrations after PRB exceeded the control standard for 80 h. However, only 7–16% of Cd remained in the pore water when the flow passed the WPWS PRB; that is, 84–93% of Cd was removed from the aquifer stream. As expected, AsO_3^{3-} penetrated the WPWS PRB more easily than the other metals. Considerable amounts of As were observed behind the WPWS PRB at any time, thereby indicating that it is difficult for the WPWS PRB to prevent the spread of As (Table 6). Negatively charged carboxylic groups in WPWS expelled AsO_3^{3-} ions. The AsO_3^{3-} mass flow seemed to advance within both the middle and bottom layers, which increased the adsorption loading

Table 4 | Dynamics of Ni^{2+} in the aquifer from the metal mixture plume (mg L^{-1})

	Site before barrier			Site after barrier		
Sampling order/time (h)	S	M	L	S	M	L
1/8	0.097	0.149	0.459	0.189	0.282	0.684
2/16	–	–	–	0.175	0.253	0.649
3/24	–	–	–	0.175	0.249	0.459
4/32	0.261	0.270	0.280	0.166	0.230	0.295
5/40	–	–	–	0.196	0.245	0.283
6/48	–	–	–	0.183	0.236	0.292
7/56	0.635	0.672	0.267	0.152	0.169	0.234
8/64	–	–	–	0.173	0.185	0.270
9/72	–	–	–	0.159	0.175	0.267
10/80	0.552	0.604	0.216	0.169	0.203	0.274
11/88	–	–	–	0.133	0.140	0.207
12/96	–	–	–	0.118	0.127	0.193
13/104	0.572	0.644	0.502	0.111	0.101	0.189
14/112	–	–	–	0.104	0.100	0.163
15/120	–	–	–	0.097	0.092	0.157
16/128	0.434	0.445	0.490	0.081	0.078	0.154
17/136	–	–	–	0.083	0.086	0.142
18/144	–	–	–	0.086	0.067	0.135
19/152	0.241	0.237	0.297	0.080	0.073	0.116
20/160	–	–	–	0.082	0.067	0.115
21/168	–	–	–	0.069	0.060	0.111
22/176	–	–	–	0.073	0.058	0.099

Numbers with a gray background: pollutant concentrations over the control standard, 0.1 mg L^{-1}.
Sampling at 8 h intervals. Sampling site, S: below the water table of 1 cm. M: half depth of the aquifer. L: 1 cm above the tank bottom.
–: No sampling.

at the lower part of the PRB. Thus, when the PRB encountered an invasion from large amounts of AsO_3^{3-}, the As concentrations behind the PRB did not meet the control standard for 80 h. Interestingly, the WPWS PRB continued to intercept high amounts of AsO_3^{3-}, with only 18 to 45% of As remaining in the flow. In summary, the average block efficiencies in this study for Cr, Cu, Zn, Ni, Cd, and As were calculated to be 96, 87, 91, 51, 94, and 62%, respectively. This indicates that WPWS showed least intercept to Ni^{2+} and AsO_3^{3-}.

Distribution of heavy metals in WPWS PRB

The residual contents of various metals in each section of the WPWS PRB are listed in Table 7. The heavy metal amounts in the second half of the PRB were clearly higher than the expected levels. A high-efficiency PRB intercepted most of the pollutants in its first half. In general, if the first half cannot capture excess pollutants, residual pollutants will accumulate in the second half and accelerate their breakthrough to the barrier. In summary, the adsorbed metal distribution in the WPWS PRB was consistent with their migration dynamics in the first sand zone. Chromium continued to show the highest amount in WPWS PRB, except for Zn. This indicates that $HCrO_4^-$ ions reacted with the organic component in PRB and rapidly transformed to Cr(III). WPWS steadily maintained Cr(III) levels, which resulted in a scarcity of $HCrO_4^-$ behind the barrier. However, the porosity of the WPWS PRB was near 0.5, so the quantities of $HCrO_4^-$ ions were fixed in the second half. This study proves that the WPWS PRB is useful in remediating Cr(VI) contamination in groundwater. Zinc had the highest accumulation amount in the WPWS PRB owing to its extremely high concentration in the original mixture solution.

Table 5 | Dynamics of Cd^{2+} in the aquifer from the metal mixture plume (mg L^{-1})

	Site before barrier			Site after barrier		
Sampling order/time (h)	S	M	L	S	M	L
1/8	ND	ND	ND	ND	ND	ND
2/16	–	–	–	ND	ND	ND
3/24	–	–	–	ND	ND	ND
4/32	0.004	0.003	ND	ND	ND	ND
5/40	–	–	–	ND	ND	ND
6/48	–	–	–	ND	ND	ND
7/56	0.093	0.088	0.010	0.011	0.019	ND
8/64	–	–	–	0.005	0.009	ND
9/72	–	–	–	0.013	0.013	0.004
10/80	0.075	0.053	0.002	0.004	0.005	ND
11/88	–	–	–	0.004	0.011	ND
12/96	–	–	–	ND	0.009	0.004
13/104	0.074	0.075	0.034	ND	0.012	0.006
14/112	–	–	–	ND	0.009	0.008
15/120	–	–	–	ND	0.003	ND
16/128	0.043	0.054	0.023	ND	0.006	0.006
17/136	–	–	–	ND	0.005	0.007
18/144	–	–	–	ND	ND	ND
19/152	0.038	0.052	0.024	ND	ND	0.002
20/160	–	–	–	ND	ND	ND
21/168	–	–	–	ND	ND	ND
22/176	–	–	–	ND	ND	0.004

Numbers with a gray background: pollutant concentrations over the control standard, 0.005 mg L^{-1}.
Sampling at 8 h intervals. Sampling site, S: below the water table of 1 cm. M: half depth of the aquifer. L: 1 cm above the tank bottom.
–: No sampling.

Compared to other metals, Zn has the least toxicity in humans. The Zn adsorption distribution was fairly uniform throughout the WPWS PRB. The PRB also intercepted high amounts of Cu, and the first half adsorbed more Cu than the other parts (1:0.85). The distribution of Ni in the WPWS PRB was non-uniform. Its content in the first half was lower than that in the second half (0.93:1). We suspected that Ni^{2+} encountered multiple competitive adsorptions from other species of cations in this area; therefore, the expelled Ni^{2+} was forced to move further and then was trapped. More Cd was observed in the first half of the experiment, as its content was approximately 1.25 times higher than that in the other part. Arsenite was the least frequently intercepted pollutant in the WPWS PRB. The residual average of As was only 2 ppm, and this amount was only up to 0.6% of $HCrO_4^-$ adsorption. This indicates that the affinity between AsO_3^{3-} and WPWS was quite small. Therefore, AsO_3^{3-} easily passed through the barrier. However, the distribution of As in the WPWS PRB was relatively uniform.

Table 8 presents the comparison of block capacity of WPWS from metallic concentration in the aquifer or in PRB for $HCrO_4^-$, Cu^{2+}, Zn^{2+}, Ni^{2+}, Cd^{2+}, and AsO_3^{3-} with that of various materials reported in literatures (Song *et al.* 2021). Clearly, the zero-valent iron exhibits more block potential for most metals. Other composite materials with a higher intercept capacity were also prepared going through a complicated process, this increasing the cost of operation. Our RPB was built to a simple structure, but it enabled relative high intercept to be shown for $HCrO_4^-$, Cu^{2+}, Zn^{2+}, and Cd^{2+}, approaching those proposed by the literatures. However, using WPWS for the PRB remediation is feasible and more economic.

Table 6 | Dynamics of AsO_3^{3-} in the aquifer from the metal mixture plume (mg L^{-1})

	Site before barrier			Site after barrier		
Sampling order/time (h)	**S**	**M**	**L**	**S**	**M**	**L**
1/8	0.036	0.061	0.279	0.102	0.098	0.141
2/16	–	–	–	0.075	0.094	0.129
3/24	–	–	–	0.063	0.075	0.111
4/32	0.114	0.163	0.125	0.054	0.068	0.063
5/40	–	–	–	0.059	0.057	0.062
6/48	–	–	–	0.048	0.052	0.065
7/56	0.121	0.161	0.222	0.036	0.043	0.061
8/64	–	–	–	0.038	0.039	0.064
9/72	–	–	–	0.036	0.044	0.068
10/80	0.076	0.175	0.157	0.040	0.045	0.070
11/88	–	–	–	0.028	0.032	0.053
12/96	–	–	–	0.020	0.025	0.049
13/104	0.113	0.204	0.214	0.023	0.023	0.053
14/112	–	–	–	0.018	0.021	0.051
15/120	–	–	–	0.017	0.017	0.041
16/128	0.051	0.080	0.130	0.015	0.016	0.048
17/136	–	–	–	0.017	0.017	0.041
18/144	–	–	–	0.015	0.014	0.034
19/152	0.042	0.029	0.065	0.016	0.016	0.033
20/160	–	–	–	0.018	0.012	0.029
21/168	–	–	–	0.013	0.013	0.029
22/176	–	–	–	0.017	0.011	0.027

Numbers with a gray background: pollutant concentrations over the control standard, 0.05 mg L^{-1}.
Sampling at 8 h intervals. Sampling site, S: below the water table of 1 cm. M: half depth of the aquifer. L: 1 cm above the tank bottom.
–: No sampling.

Table 7 | Distribution of adsorbed metal ions in the WPWS PRB

	Cr	Cu	Zn	Ni	Cd	As
Zones in barrier	**ppm**					
F5, S5	296 ± 4, 347 ± 15	172 ± 9, 191 ± 13	1,625 ± 26, 1,630 ± 30	132 ± 10, 112 ± 8	16.0 ± 0.9, 12.0 ± 0.2	2.1 ± 0.3, 1.4 ± 0.1
F4, S4	218 ± 7, 432 ± 18	310 ± 20, 211 ± 14	1,600 ± 29, 1,615 ± 21	137 ± 6, 216 ± 7	19.5 ± 0.8, 15.0 ± 0.6	2.2 ± 0.1, 2.1 ± 0.1
F3, S3	448 ± 21, 321 ± 16	261 ± 11, 148 ± 8	1,600 ± 25, 1,630 ± 18	235 ± 13, 168 ± 11	17.5 ± 0.9, 10.0 ± 0.7	1.1 ± 0.1, 2.1 ± 0.3
F2, S2	349 ± 16, 395 ± 21	192 ± 13, 181 ± 13	1,630 ± 17, 1,610 ± 22	132 ± 5, 199 ± 13	12.5 ± 0.3, 13.5 ± 0.4	2.3 ± 0.2, 2.3 ± 0.3
F1, S1	337 ± 10, 424 ± 15	117 ± 16, 167 ± 10	1,615 ± 14, 1,495 ± 17	186 ± 10, 186 ± 11	14.0 ± 0.6, 13.0 ± 0.5	2.3 ± 0.4, 2.2 ± 0.3
Average	330 364	210 179	1,614 1,596	164 176	15.9 12.7	2.0 2.0

F, First half of WPWS barrier; S, Second half of WPWS barrier.

Table 8 | A comparison of intercept capacity of experimented metal for various materials under similar operational condition

Pollutant	PRB material	Time	Condition of removal	Initial conc.	Intercept rate	Adsorption (mg/g)	Literature
$HCrO_4^-$	Bioactive sand	50 min	Length: 30 cm; diameter: 3.75 cm; 480 g silica sand; pore volume: 104 mL; 12 mL/min	0.52 mg/L	100%		Han *et al.* (2016)
	cellulomonas sp. Strain ES6	120 d	Length: 17 cm; diameter: 2.5 cm; 1.32 mL/h	2 mg/L	100%		Viamajala *et al.* (2008)
	WPWS	176 h	Thickness: 10 cm; height: 70 cm; width: 50 cm; 243 mL/min	0.25 mg/L	96%	0.347	This work
Cu^{2+}	Mixture of municipal compost and calcite	16 h	Length: 50 cm; diameter: 5 cm; porosity: 0.5; 0.5 mL/min	16 mg/L	>99%		Gibert *et al.* (2005)
	EGDE–CS–NZVI beads	6 h	Length: 50 cm; diameter: 1.5 cm ; 35.6 cm adsorbent filling; 60 mL/h; pH: 6.4	10 mg/L	>96%	67.2	Liu *et al.* (2013)
	Mixture of limestone, vegetal compost and ZVI cutting	36 mon	Thickness:140 cm, parallel to groundwater flow; width: 30 m long perpendicular to groundwater flow; average 6.0 m deep; 0.5–1 m/d	1.2 mg/L	76%		Gibert *et al.* (2011)
	WPWS	176 h	Thickness: 10 cm; height: 70 cm; width: 50 cm; 243 mL/min	5 mg/L	87%	0.195	This work
Zn^{2+}	Acid-washed ZVI/ ZVAl mixtures	20 d	Length: 45 cm; diameter: 5 cm; height of filled sorbent: 5 cm; pH 5.4; 1.0 mL/min; acid-washed ZVI/ZVAl: 80 g/40 g	20 mg/L	99.5%		Han *et al.* (2016)
	Mixture of limestone and vegetal compost	36 mon	Thickness: 140 cm, parallel to groundwater flow; width: 30 m, perpendicular to groundwater flow; average 6.0 m deep; 0.5–1 m/d	20 mg/L	47%		Gibert *et al.* (2011)
	Mixture NZVI and pumice	17 d	Length: 50 cm; diameter: 5 cm; 0.5 mL/ min	23 mg/L	94.2%	13.6	Bilardi *et al.* (2013)
	WPWS	176 h	Thickness: 10 cm; height: 70 cm; width: 50 cm; 243 mL/min	25 mg/L	91%	1.605	This work
Ni^{2+}	ZVI/zeolite/ activated carbon mixture	92.7 h	Weight ratio of ZVI, zeolite and activated carbon: 5:1:4; porosity: 43.2%; 0.5 mL/min	0.73 mg/L	70.7%		Zhou *et al.* (2014)
	Pervious concrete	1 d	Length: 50 cm; diameter: 10 cm; 0.35 mL/min	1.3 mg/L	69.2%		Shabalala *et al.* (2017)
	WPWS	176 h	Thickness: 10 cm; height: 70 cm; width: 50 cm; 243 mL/min	0.5 mg/L	51%	0.17	This work
Cd^{2+}	Corn straw, fly ash, zeolite, and Fe-Mn nodule mixture	1 h	Length: 20 cm; diameter: 5 cm; quartz sand: corn straw: synthesized zeolites: fly ash: iron-manganese nodule: quartz sand (in sequence) = 1: 2: 2: 2: 2: 2 (volume); 6 mL/min	0.5 mg/L	97%		Fan *et al.* (2018)
	Compost, ZVI, limestone gravel, and granite pea gravel mixture	30 mon	Thickness:7.9 m, depth: 4.1 m, width: 1.8 m; 30% (v/v) leaf/yard compost, 20% (v/v) ZVI, 5% (v/v) limestone gravel, 45% (v/v) granite pea gravel; average hydraulic gradient: 0.002	1.44 mg/L	99.9%		Ludwig *et al.* (2009)

(*Continued*)

Table 8 | Continued

Pollutant	PRB material	Time	Condition of removal	Initial conc.	Intercept rate	Adsorption (mg/g)	Literature
	EGDE–CS–NZVI beads	6 h	Length: 50 cm, diameter: 1.5 cm; 35.6 cm adsorbent filling; 60 mL/h; pH 6.4	10 mg/L	>96%		Liu *et al.* (2013)
	WPWS	176 h	Thickness: 10 cm; height: 70 cm; width: 50 cm; 243 mL/min	0.025 g/L	94%	0.0143	This work
AsO_4^{3-}	6% leaves, 9% compost, 3% Fe(0), 30% Si sand, 30% perlite, 22% limestone mixture (w/w %)	18 mon	Thickness: 80 cm, diameter: 20 cm; 0.5 mL/min	2 mg/L	99%	517	Viggi *et al.* (2010)
AsO_3^{3-}	ZVI bound with aluminosilicate	3 yr	0.3–6 L/min	0.21 mg/L	98.9%		Morrison *et al.* (2002)
	WPWS	176 h	Thickness: 10 cm; height: 70 cm; width: 50 cm; 243 mL/min	0.25 mg/L	62%	0.002	This work

ZVI, zero-valent iron; ZVAl, zero-valent aluminum; NZVI, nano-ZVI; EGDE, ethylene glycol diglycidyl ether.

CONCLUSIONS

A WPWS PRB may weaken the hazards from $HCrO_4^-$, Cu^{2+}, and Zn^{2+} in a simulated aquifer, but it was unable to prevent the dispersal of AsO_3^{3-}, Ni^{2+}, and Cd^{2+}. These results may be attributed to the slight hydrophobicity of the WPWS, which caused a decrease in the water permeability of the WPWS PRB. However, the sand layer showed significant adsorption of positively charged heavy metals, large amounts of metal cations were fixed in the zone. Two kinds of competitive adsorption are speculated to have occurred in this system, including adsorptive competition between heavy metals and sands, as well as adsorptive competition between heavy metals and WPWS. The effect of multiple competitive adsorption on Ni^{2+} enhanced the formation of the high concentration Ni^{2+} mass flow in the sand layer, which eventually led to a failure in the block.

A WPWS can feasibly be utilized to create a PRB for remediation in a brown field, although it did not block all the metals in this study. There are three reasons for this: (1) the effect of competitive adsorption, (2) conducting the experiment under a super high concentrations, and (3) the experiment utilized a PRB only 10 cm thick. Brown field plumes rarely contain more than three species of metals, and metal concentrations are usually not as high as those tested in this study. When remediation in a brown field concludes, we suggest digging up the WPWS PRB and sending its debris to a brick kiln factory or a cement factory for final disposal. The Fe, Al, Ca, and Si in the WPWS may serve as raw materials for producing bricks or cement. Toxic metals trapped in WPWS particles would then be sintered and fixed into the structure of brick or cement, and their toxicity would hence be removed.

ACKNOWLEDGEMENTS

This work was financially supported by the Environmental Protection Administration Executive Yuan, Republic of China, under Project 109C003913.

DATA AVAILABILITY STATEMENT

All relevant data are included in the paper or its Supplementary Information.

REFERENCES

Ahuja, S. 2008 *Arsenic Contamination of Groundwater: Mechanism, Analysis, and Remediation*. John Wiley & Sons Hoboken, NJ.

ATSDR, Agency for Toxic Substances and Disease Registry 2007 *Toxicological Profile for Arsenic*. PHS (August 2007). U.S. Department of Health and Human Services, Washington, DC.

Avom, J., Mbadcam, J. K., Noubactep, C. & Germain, P. 1997 Adsorption of methylene blue from an aqueous solution onto activated carbon from palm-tree cobs. *Carbon* **35** (3), 365–369.

Bilardi, S., Calabro, P. S., Care, S., Moraci, N. & Noubactep, C. 2013 Improving the sustainability of granular iron/pumice systems for water treatment. *Journal of Environmental Management* **121**, 133–141.

Chen, L., Liu, F. Y., Liu, L., Dong, H. Z. & Colberg, P. J. S. 2011 Benzene and toluene biodegradation down gradient of a zero-valent iron permeable reactive barrier. *Journal of Hazardous Materials* **188**, 110–115.

Chen, K. Y., Tzou, Y. M., Chan, Y. T., Wu, J. J., Teah, H. Y. & Liu, Y. T. 2019 Removal and simultaneous reduction of Cr(VI) by organo-Fe(III) composites produced during coprecipitation and coagulation processes. *Journal of Hazardous Materials* **376**, 12–20.

Czurda, K. A. & Haus, R. 2002 Reactive barriers with fly ash zeolites for in situ groundwater remediation. *Applied Clay Science* **21**, 13–20.

Dhal, B., Thatoi, H. N., Das, N. N. & Pandey, B. D. 2013 Chemical and microbial remediation of hexavalent chromium from contaminated soil and mining/metallurgical solid waste: a review. *Journal of Hazardous Materials* **250–251**, 272–291.

Dong, J., Zhao, Y. S., Zhang, W. H. & Hong, M. 2009 Laboratory study on sequenced permeable reactive barrier remediation for landfill leachate-contaminated groundwater. *Journal of Hazardous Materials* **161**, 224–230.

Erto, A., Lancia, A., Bortone, I., Di Nardo, A., Di Natale, M. & Musmarra, D. 2011 A procedure to design a permeable adsorptive barrier (PAB) for contaminated groundwater remediation. *Journal of Environmental Management* **92**, 23–30.

Fan, C., Gao, Y., Zhang, Y., Dong, W. & Lai, M. 2018 Remediation of lead and cadmium from simulated groundwater in loess region in northwestern China using permeable reactive barrier filled with environmentally friendly mixed adsorbents. *Environmental Science and Pollution Research* **25**, 1486–1496.

Gavaskar, A. R. 1999 Design and construction techniques for permeable reactive barriers. *Journal of Hazardous Materials* **68**, 41–71.

Gibert, O., Pablo, J. D., Cortina, J. L. & Ayora, C. 2005 Municipal compost-based mixture for acid mine drainage bioremediation: metal retention mechanisms. *Applied Geochemistry* **20** (9), 1648–1657.

Gibert, O., Rötting, T., Cortina, J. L., Pablo, J. D., Ayora, C., Carrera, J. & Bolzicco, J. 2011 In-situ remediation of acid mine drainage using a permeable reactive barrier in Aznalcóllar (Sw Spain). *Journal of Hazardous Materials* **191** (1–3), 287–295.

Guerin, T. F., Horner, S., McGovern, T. & Davey, B. 2002 An application of permeable reactive barrier technology to petroleum hydrocarbon contaminated groundwater. *Water Research* **36**, 15–24.

Han, W., Fu, F., Cheng, Z., Tang, B. & Wu, S. 2016 Studies on the optimum conditions using acid-washed zero-valentiron/aluminum mixtures in permeable reactive barriers for the removal of different heavy metal ions from wastewater. *Journal of Hazardous Materials* **302**, 437–446.

Henderson, A. D. & Demond, A. H. 2007 Long-term performance of zero-valent iron permeable reactive barriers: a critical review. *Environmental Engineering Science* **24**, 401–423.

Hillel, D. 1999 Soil and hydrologic cycle. In: *The Nature and Properties of Soils*, 12th edn (Brady, N. C. & Weil, R. R., eds). Prentice-Hall, Inc., Upper Saddle River, New Jersey, pp. 213–264.

Hu, B., Song, Y., Wu, S., Zhu, Y. & Sheng, G. 2019a Slow released nutrient-immobilized biochar: a novel permeable reactive barrier filler for Cr (VI) removal. *Journal of Molecular Liquids* **286**, 110876.

Hu, Y., Zhang, M. & Li, X. 2019b Improved longevity of nanoscale zero-valent iron with a magnesium hydroxide coating shell for the removal of Cr(VI) in sand columns. *Environment International* **133**, 105249.

Kim, H. S., Kim, Y. J. & Seo, Y. R. 2015 An overview of carcinogenic heavy metal: molecular toxicity mechanism and prevention. *Journal of Cancer Prevention* **20** (4), 232–240.

Komárek, M., Vaněk, A. & Ettler, V. 2013 Chemical stabilization of metals and arsenic in contaminated soils using oxides – a review. *Environmental Pollution* **172**, 9–22.

Kumarasinghe, U., Kawamoto, K., Saito, T., Sakamoto, Y. & Mowjood, M. I. M. 2018 Evaluation of applicability of filling materials in permeable reactive barrier (PRB) system to remediate groundwater contaminated with Cd and Pb at open solid waste dump sites. *Process Safety and Environmental Protection* **120**, 118–127.

Liu, C. C., Wang, M. K. & Li, Y. S. 2005 Removal of nickel from aqueous solution using wine processing waste sludge. *Industrial & Engineering Chemistry Research* **44**, 1438–1445.

Liu, C. C., Wang, M. K., Li, Y. S., Chiou, C. S., Lin, Y. A. & Huang, S. S. 2006 Chromium removal and sorption mechanism from aqueous solutions by wine processing waste sludge. *Industrial & Engineering Chemistry Research* **45**, 8891–8899.

Liu, C. C., Wang, M. K., Chiou, C. S., Li, Y. S. & Lin, Y. A. 2009 Biosorption of chromium, copper and zinc by wine-processing waste sludge: single and multi-component system study. *Journal of Hazardous Materials* **171**, 386–392.

Liu, C. C., Li, Y. S., Chen, Y. M., Wang, M. K., Chiou, C. S., Yang, C. Y. & Lin, Y. A. 2011 Biosorption of chromium, copper and zinc on rice wine processing waste sludge in fixed bed. *Desalination* **267**, 20–24.

Liu, C. C., Chen, Y. M., Wang, M. K. & Lin, Y. A. 2012a Adsorption of Cu(II) from aqueous solution by wine processing waste sludge. *Water Environment Research* **84** (9), 733–743.

Liu, J. P., Zhang, H. Z. & Liu, X. M. 2012b Commercial activated carbon modified with sulfuric acid: a potential permeable reactive barrier material for in situ remediation of Cr(VI) from groundwater. *Advanced Materials Research* **343–344**, 172–176.

Liu, T., Yang, X., Wang, Z. & Yan, X. 2013 Enhanced chitosan beads-supported Fe(0)-nanoparticles for removal of heavy metals from electroplating wastewater in permeable reactive barriers. *Water Research* **47** (17), 6691–6700.

Liu, C. C., Liu, Y. C. & Liu, J. Y. 2020 Wine-processing waste sludge permeable reaction barrier utilized to block a gasoline plume in a simulated aquifer. *Water Science & Technology* **82** (7), 1304–1310.

Logan, W. B. 1999 Soil colloid their nature and practical significance. In: *The Nature and Properties of Soils*, 12th edn (Brady, N. C. & Weil, R. R., eds) Prentice-Hall, Inc., Upper Saddle River, New Jersey, pp. 307–342.

Ludwig, R. D., Smyth, D. J. A., Blowes, D. W., Spink, L. E., Wilkin, R. T. & Jewett, D. G. 2009 Treatment of arsenic, heavy metals, and acidity using a mixed ZVI-compost PRB. *Environmental Science & Technology* **43** (6), 1970–1976.

Maamoun, I., Eljamal, O., Falyouna, O., Eljamal, R. & Sugihara, Y. 2020 Multi-objective optimization of permeable reactive barrier design for Cr(VI) removal from groundwater. *Ecotoxicology and Environmental Safety* **200**, 110773.

McBride, M. 1989 Reactions controlling heavy metal solubility in soils. *Advances in Soil Science* **10**, 1–56.

Mittal, A., Singh, R., Chakma, S., Goel, G. & Birke, V. 2021 An integrated permeable reactive barrier and photobioreactor approach for simultaneous removal of nitrate, phosphate and hexavalent chromium: a combined batch and continuous flow study. *Bioresource Technology* **333**, 125201.

Morrison, S. J., Metzler, D. R. & Dwyer, B. P. 2002 Removal of As, Mn, Mo, Se, U, V and Zn from groundwater by zero-valent iron in a passive treatment cell: reaction progress modeling. *Journal of Contaminant Hydrology* **56** (1/2), 99–116.

Nur-E-Alam, M., Mia, M. A. S., Ahmad, F. & Rahman, M. M. 2020 An overview of chromium removal techniques from tannery effluent. *Applied Water Science* **10**, 205.

Obiri-Nyarko, F., Grajales-Mesa, S. J. & Malina, G. 2014 An overview of permeable reactive barriers for in situ sustainable groundwater remediation. *Chemosphere* **111**, 243–259.

Okyere, M. S. 2019 *Corrosion Protection for the Oil and Gas Industry: Pipelines, Subsea Equipment, and Structures*. CRC Press, Boca Raton, FL.

Rent, G., Wang, X., Huang, P., Zhong, B., Zhang, Z., Yang, L. & Yang, X. 2017 Chromium (VI) adsorption from wastewater using porous magnetite nanoparticles prepared from titanium residue by a novel solid-phase reduction method. *Science of the Total Environment* **607–608**, 900–910.

Shabalala, A. N., Ekolu, S. O., Diop, S. & Solomon, F. 2017 Previous concrete reactive barrier for removal of heavy metals from acid mine drainage-column study. *Journal of Hazardous Materials* **323**, 641–653.

Singh, A. K. & Singh, K. P. 2018 Optimization of phosphate removal from aqueous solution using activated carbon supported zero-valent iron nanoparticles: application of RSM approach. *Applied Water Science* **8**, 226.

Snape, I., Morris, C. E. & Cole, C. M. 2001 The use of permeable reactive barriers to control contaminant dispersal during site remediation in Antarctica. *Cold Regions Science and Technology* **32** (2–3), 157–174.

Song, J., Huang, G., Han, D., Hou, Q., Gan, L. & Zhang, M. 2021 A review of reactive media within permeable reactive barriers for the removal of heavy metal(loid)s in groundwater: current status and future prospects. *Journal of Hazardous Materials* **319**, 128644.

Statham, T. M., Stark, S. C., Snape, I., Strvens, G. W. & Mumford, K. A. 2016 A permeable reactive barrier (PRB) media sequence for the remediation of heavy metal and hydrocarbon contaminated water: a field assessment at Casey Station, Antarctica. *Chemosphere* **147**, 368–375.

Viamajala, S., Peyton, B. M., Gerlach, R., Sivaswamy, V. & Petersen, J. N. 2008 Permeable reactive biobarriers for in situ Cr(VI) reduction: bench scale tests using *cellulomonas* sp. strain ES6. *Biotechnology & Bioengineering* **101** (6), 1150–1162.

Viggi, C. C., Pagnanelli, F., Cibati, A., Uccelletti, D., Palleschi, C. & Toro, L. 2010 Biotreatment and bioassessment of heavy metal removal by sulphate reducing bacteria in fixed bed reactors. *Water Research* **44**, 151–158.

Walkley, A. J. & Black, I. A. 1934 Estimation of soil organic carbon by the chromic acid titration method. *Soil Science* **37**, 29–38.

Wei, X., Kong, X., Wang, S., Xiang, H., Wang, J. & Chen, J. 2013 Removal of heavy metals from electroplating wastewater by thin-film composite nanofiltration hollow-fiber membranes. *Industrial & Engineering Chemistry Research* **52** (49), 17583–17590.

Wu, B. 2020 Chapter 6 - Human health hazards of wastewater. In: (Ren, H. & Zhang, W., eds), High-Risk Pollutants in Wastewater. Elsevier, Amsterdam, The Netherlands, pp. 125–139.

Yuan, G. L., Sun, T. H., Han, P., Li, J. & Lang, X. X. 2014 Source identification and ecological risk assessment of heavy metals in topsoil using environmental geochemical mapping: typical urban renewal area in Beijing, China. *Journal of Geochemical Exploration* **136**, 40–47.

Zhou, D., Yan, L., Zhang, Y., Chang, Z., Li, X. & Chen, Z. 2014 Column test-based optimization of the permeable reactive barrier (PRB) technique for remediating groundwater contaminated by landfill leachates. *Journal of Contaminant Hydrology* **168**, 1–16.

First received 21 June 2021; accepted in revised form 20 September 2021. Available online 5 October 2021